Optimal Relay Placement in Two-Hop RF Energy Transfer

Deepak Mishra and Swades De

***Abstract*—Recently, wireless radio frequency energy transfer (RFET) has emerged as an effective technology for prolonging lifetime of the energy-limited wireless sensor networks. However, low RFET efficiency is still a fundamental bottleneck in its widespread usage. Multi-hop RF energy transfer (MHET) can improve the RFET efficiency by deploying relay nodes that scavenge the dispersed energy and transfer it to the nearby sensor node. The efficiency of MHET is strongly influenced by the relay node's placement. To maximize the RFET efficiency for a two-hop scenario, in this paper a novel optimization model is proposed to determine the optimal relay placement (ORP) on an Euclidean $x-y$ plane. Nontrivial tradeoff between the energy scavenged at the relay versus the effective energy delivered by the relay to the target node is investigated. Due to the nonconvex and highly nonlinear nature of the optimization problem, an α-based branch and bound algorithm has been used. The proposed optimization model is further extended by incorporating distributed beamforming to enhance the RFET efficiency. Numerical results illustrate that the proposed algorithm provides convergence to the ϵ-global optimal solution in a few iterations, and ORP provides significant energy saving over arbitrary relay positions for commercial RF energy harvesting systems.**

***Index Terms*—RF energy harvesting; two-hop RF energy transfer; optimal relay placement; energy transfer efficiency; distributed beamforming**

I. Introduction and motivation

Finite energy storage capacity of the field nodes in wireless sensor network (WSN) is one of the major bottlenecks to its large-scale deployment. Wireless energy transfer using dedicated radio frequency (RF) energy source has the potential to provide uninterrupted network operation by recharging the sensor nodes on demand [1]. However, like wireless information transfer, RF energy transfer (RFET) also suffers from various losses, including path loss, energy dissipation, shadowing, and fading. Moreover, due to the restrictions of maximum transmitter power and receiver sensitivity, energy transfer efficiency is an important and formidable issue in RFET. Novel techniques for boosting the energy transfer efficiency and saving energy are very essential from the perspectives of energy-constrained WSNs and green communication systems.

A. Prior art and motivation

Multi-hop RFET (MHET) can improve the energy harvesting efficiency with the help of relay nodes nearby the target node. The gain in MHET is achieved by collecting the otherwise-dispersed RF energy of the source and transferring it to the target node with reduced path loss. RF-to-DC conversion efficiency is improved due to higher received power. There have been only a few works reported on multi-hop energy transfer [1]–[6]. In [2], a non-radiative multi-hop energy transfer has been explored. Perpetual Wireless Networks fueled by multi-hop wireless distribution of injected power was considered in [3]. In [4], an optimization model was proposed to determine the minimum number of chargers needed to recharge the nodes of a network in a multi-hop fashion. However, in [3], [4], a non-radiative form of energy transfer based on resonant magnetic induction was used.

Unlike non-radiative wireless transfer of energy, radiative RFET does not have the strong alignment, coupling, and limited range constraints [7]. Also, RFET has the advantages of beam steering, simultaneous charging of multiple nodes, and combining data and energy transfer over the same RF signal [1], [8]. In [1], a feasibility study of MHET was conducted, where it was demonstrated that under certain optimum distance conditions, MHET is efficient in terms of both energy and time. Two-hop RFET (2HET) was experimentally demonstrated in [5]. It was also shown that, for a higher RFET efficiency, relay node's position closer to RF source or closer to target node are better than the center. In [6], experimental demonstration of RFET over multiple multi-hop paths other than direct energy transfer (DET) was conducted in both sparse and dense network scenarios. The studies in [5], [6] however did not quantitatively investigate the optimal relay placement (ORP). Since the improvement in RFET efficiency provided by MHET is strongly influenced by the relay placement, here we investigate the ORP problem in 2HET.

Optimal power allocation and relay location strategies for cooperative communication using amplify-and-forward (AF) and decode-and-forward (DF) information relays under different fading conditions were studied in [9]–[12]. There also have been a few works on cooperative relaying for simultaneous wireless information and power transfer (SWIPT) [13], [14]. The study in [14] claimed that there exists a tradeoff between information transfer and energy transfer for relay selection in SWIPT, because the preferable relay positions are different for the two objectives. The relay node in [9]–[14] is assumed externally powered or self-powered, whereas in MHET the relay node is powered by collecting the dispersed energy of the RF source. In [15], two practical relaying protocols based on time switching (TS) and power splitting (PS) architectures were proposed for energy harvesting AF relay node with one source-destination pair. The objectives were to optimize the outage probability and the ergodic capacity in delay-limited as

D. Mishra and S. De are with the Department of Electrical Engineering and Bharti School of Telecommunication, Indian Institute of Technology Delhi, New Delhi, India. E-mail: {deepak.mishra, swadesd}@ee.iitd.ac.in.

This work was supported by the Department of Electronics and Information Technology under Grant 13(2)/2012-CC&BT.

well as in delay-tolerant modes. Considering multiple source-destination pairs and a single DF relay node, four PS strategies for energy harvesting relay were proposed in [16] to efficiently distribute the power harvested at the relay among the multiple users. While [15] and [16] considered the usage of energy harvesting relay for two-hop information transfer with no direct communication link between the source and destination, in our current work we use the energy harvesting relay for two-hop energy transfer along with the available DET link.

It may be noted that, ORP for energy transfer is different from the conventional ORP and relay selection techniques for information transfer. Firstly, the information reception sensitivity is much higher than the energy reception sensitivity by a few orders of magnitude (typically -60 dBm in data reception versus -10 dBm in energy reception). Secondly, the metric to be optimized in ORP for information transfer is signal-to-noise ratio (SNR) at the receiver or symbol error probability (SEP), whereas in energy transfer the objective function is to maximize the received power or energy transfer efficiency. Thirdly, information relaying can be two way [9], whereas energy relaying is generally one way only. *To our best knowledge, this is the first work that investigates ORP for efficient RFET, where the relay node is powered by the energy scavenged from the RFET to the target node.*

A distributed beamforming approach was proposed in [17] for data transfer with increased rate and transmission range. Fully wireless distributed beamforming prototype based on a software defined radio platform was also proposed in [18], where frequency and phase synchronizations were achieved using extended Kalman filtering and a one-bit feedback. Multi-antenna techniques have been introduced recently for improving the energy transfer efficiency by beamforming [19]. In [20], it was shown that collective transmission from multiple sources can provide significant gain over DET by distributed beamforming. In our work, cooperative energy transfer from the RF source and relay differs from [20] in that, here the relay transfers energy in store-and-forward fashion and the effective relayed energy is strongly influenced by its placement.

B. Contributions

Motivated by the experimental results in [5], [6], and the observations in [1], [18], [20], in this work we investigate the ORP problem in 2HET in 2-D Euclidean space that aids RFET without affecting the DET under a given set of device or system parameters, such as RF source to target distance, antenna characteristics, RF-to-DC conversion efficiency, and store-and-forward energy transfer. This optimization problem is nonconvex and highly nonlinear. So α-based Branch and Bound (αBB) algorithm [21] is employed to solve the problem up to some predefined acceptable tolerance ϵ. We also utilize cooperative or distributed beamforming of the RF source and relay node to further improve the energy transfer efficiency. The contribution of this work is four-fold:

i) It provides an analytical model for store-and-forward energy transfer with the relay node powered by the energy scavenged from RF source, by deriving the expressions for constant power charging in RC parallel circuit.
ii) An optimization model is formulated for ORP in 2-D Euclidean space for 2HET and a modified αBB algorithm is proposed to find a fast ϵ-global optimal solution.
iii) A novel 1-D optimization model for ORP using distributed beamforming is proposed that offers improved 2HET efficiency with faster convergence to ORP solution.
iv) The impact of ORP with commercial RF energy harvester and antennas from Powercast [22] in terms of significant energy savings is discussed via numerical results.

C. Paper organization

We present the system model in Section II. 2HET process is characterized in Section III. In Section IV, we introduce the ORP problem in 2HET without affecting DET, and propose an application of distributed beamforming in ORP for higher RFET efficiency. In Section V, we propose a modified αBB algorithm to solve the nonconvex ORP problems. Performance gain of the proposed algorithms are captured with numerical examples in Section VI. Section VII concludes the paper.

II. 2HET System Model

A. 2HET system configuration

We consider a wireless 2HET scenario, where the location of the RF source denoted by $\mathcal{S}$ on an Euclidean $x-y$ plane is given by $(x_1, y_1) = (0, 0)$ and the location of the target sensor node $\mathcal{T}$ (energy receiver) is given by $(x_T, y_T) = (x_0, 0)$. So x_0 is the line-of-sight (LOS) distance between $\mathcal{S}$ and $\mathcal{T}$. The position of relay node $\mathcal{R}$ is unknown, which has to be determined to maximize the energy transfer efficiency. The network topology considered is shown in Fig. 1.

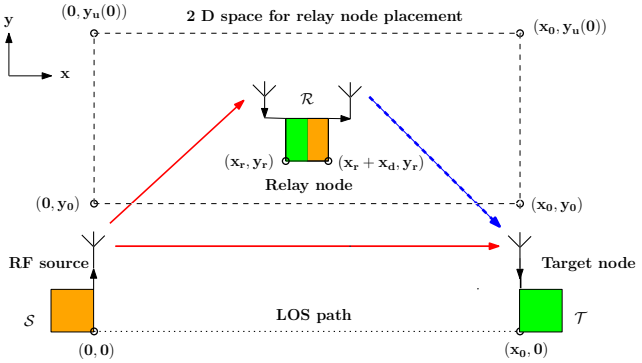

Fig. 1: Three node network topology.

Relay node comprises of two parts: a) receiver, with location (x_r, y_r) facing $\mathcal{S}$; b) transmitter, placed x_d distance away from receiver, at $(x_2, y_2) = (x_r + x_d, y_r)$ facing $\mathcal{T}$. The target node is a part of static or quasi-static wireless sensor network, powered by the energy stored in the rechargeable battery or super-capacitor and can be used for various sensing applications, such as, environment monitoring, water quality monitoring, surveillance, and disaster management.

It may be noted that, due to finite antenna size at $\mathcal{S}$, $\mathcal{R}$, and $\mathcal{T}$, to ensure that DET is unaffected by the presence of $\mathcal{R}$, it is positioned away from the LOS path between $\mathcal{S}$ and $\mathcal{T}$. To find non-blocking position of $\mathcal{R}$, we assume that y_0

is the distance of $\mathcal{R}$ from the LOS path for DET from $\mathcal{S}$ to $\mathcal{T}$. This distance y_0 depends on many parameters such as, the source power, radiation pattern of the source and target node antennas, distance x_0 between RF source and target node, and physical properties of the relay node, e.g., reflection coefficient, antenna cross-section area. y_0 can be determined experimentally through trial runs. However, to determine this position as a function of the given set of system parameters, it is required to account for scattering, reflection, and blocking, which make the ORP formulation highly complicated. Our aim is to determine the ORP that can fully utilize the advantage of 2HET in improving the energy transfer efficiency.

It may be noted from Fig. 1 that 2HET comprises of DET (single hop). We define energy transfer efficiency η_E as the improvement provided in 2HET over the DET without $\mathcal{R}$,

$$\eta_E = \left(\frac{E_{2HET} - E_{DET}}{E_{DET}}\right) \times 100 = \left(\frac{P_{2HET} - P_{DET}}{P_{DET}}\right) \times 100 \tag{1}$$

where E_{2HET}, P_{2HET}, E_{DET}, and P_{DET} are the energy and power received at $\mathcal{T}$ in 2HET and DET, respectively.

Transmissions from the RF source and the relay are considered to be at the same frequency due to the following issues: (a) Maximum energy efficiency of wireless power transfer is achieved with a single-frequency sinusoid. (b) Commercial RF energy harvesters from Powercast, that have been used in our experimental verification, operate in the range of 902-928 MHz, with reduced RF-to-DC conversion efficiency outside this band. So, using different frequency for transmissions from the RF source and the relay node will require different energy harvesters at the target node, thus incurring extra hardware cost. (c) Since the sensitivity band of commercial harvesters is very narrow, only a small frequency separation is possible, which in turn is not sufficient to avoid destructive interference.

Also, as shown in Section VI, ORP with same frequency can provide efficient RFET due to constructive interference of the energy signals received from the RF source and the relay.

Next, we explain the operation of the relay node.

B. Discontinuous transmission of energy relay node

The target node receives power from the RF source continuously. However, the transmission from the relay node is discontinuous, because energy relay node does not have a dedicated external energy supply; it is operated by the energy harvested from the radiation from the RF source that is primarily directed to the target node. Being closer to the RF source, it first harvests the energy from the RF source more efficiently than the target node, stores it in a super-capacitor or battery, and then transmits it to the target node in the form of dummy 'data' packets. Thus, there is a continuous cycle of *transmission (ON* or *active)* state and *no transmission (OFF)* state in the relay node, as shown in Fig. 2(a). During *ON* state, the relay node transmits energy to the target node until its stored energy reduces to a minimum threshold. During *OFF* state, the communication module of the relay node goes into sleep mode to allow itself recharge its drained storage element so that it can again re-transmit during the next *ON* state. Hardware implementation of RF energy relaying in *ON-OFF* mode was reported in [6]. Analytical characterization of the relay operation is presented in Section III-C. It should be noted that, as the relay node has two separate antennas – one for reception of RF energy and the other for its transmission, it can continuously harvest energy from the RF source, though it transmits in bursts only during the *ON* state. Accordingly, the duty cycle of relay node's transmission with T_{ON} and T_{OFF} as the *ON* and *OFF* state durations, respectively, is given by:

$$D_c(x_r, y_r) = \frac{T_{\text{ON}}(x_r, y_r)}{T_{\text{ON}}(x_r, y_r) + T_{\text{OFF}}(x_r, y_r)}. \tag{2}$$

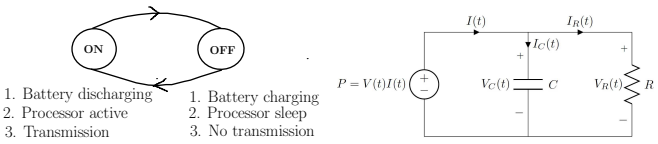

(a) ON-OFF state model (b) Equivalent RC parallel circuit

Fig. 2: Analytical model for relay node.

III. Characterization of 2HET Process

In this section, analytic model for characterization of RF charging time at the relay and target node is provided along with the derivation of the mean power received at target node.

A. Constant power charging in RC parallel circuit

Intuitively, the relay node consumes a different (higher) amount of current during *ON* state as compared to *OFF* state. So, we model the transmitter module of the energy relay node by a resistive load of different values [23] in the *ON* and *OFF* states. This resistive load is driven by the RF energy harvested and stored in the super-capacitor. Hence, the relay node can be modeled as an equivalent parallel RC circuit as shown in Fig. 2(b). *OFF* state is represented by a high resistance value R_{dch} because of low current consumption during sleep or no-transmission state. This allows most of the current coming from the source to pass through capacitor, thus charging it. So, $I_R(t) = I(t) - I_C(t)$. On the other hand, *ON* state is represented by a low resistance value R_{ch} to allow more current flowing through the load, which comes both from capacitor (discharging or *ON* state) and constant power source. So, in this case, $I_R(t) = I(t) + I_C(t)$ (direction of $I_C(t)$ gets reversed of as shown in Fig. 2(b)). The current flow is reversed in *ON* state to make up for the increased current requirement during the *energy transmission (ON)* state, because the constant power source alone cannot meet the current requirement in this state. The values of 'R' (R_{ch} and R_{dch}) have to be determined experimentally by measuring them based on the consumption of the energy transfer unit of the relay node during the deep sleep (OFF or charging) state and active (ON or discharging) state, respectively.

Charging of a super-capacitor from a constant power source is different from the conventional *constant voltage* charging. This is because the DC power used to charge the super-capacitor after RF to DC conversion of the received RF power at the receiver is fixed for a RF source transmitting constant

power from a fixed distance. We characterize the charging time of a capacitor in RC parallel circuit in order to find the charging and discharging times, which are required to find the duty cycle D_c of the relay node. It should be noted that the super-capacitors used for RF energy harvesting generally have very low ESR (on the order of mΩ), which has been neglected to obtain a simplified closed form expression. From Fig. 2(b),

$$\begin{aligned} P &= V(t)\cdot I(t) = V_C(t)\cdot[I_C(t)+I_R(t)] \\ &= \frac{q}{C}\cdot\left[\frac{dq}{dt}+\frac{q}{RC}\right] \\ \frac{dq}{dt} &= \frac{PC}{q}-\frac{q}{RC}. \end{aligned} \tag{3}$$

Solving (3) for t by integration, where, as t goes from 0 to T, charge stored in the capacitor increases from Q_i to Q,

$$T = \frac{1}{2}RC\log\left(\frac{PRC^2-{Q_i}^2}{PRC^2-Q^2}\right). \tag{4}$$

Also, solving (3) for q, we have the solution for $Q(t)$ as:

$$Q(t)=\sqrt{PRC^2\left(1-e^{\frac{-2t}{RC}}\right)+{Q_i}^2e^{\frac{-2t}{RC}}}. \tag{5}$$

Note that, in (5) Q has been replaced by $Q(t)$, because it denotes the charge on the capacitor at time t. As $Q=CV_C$, the voltage across the capacitor at time t is:

$$V_C(t)=\frac{\sqrt{PRC^2\left(1-e^{-\frac{2t}{RC}}\right)+(Q_i)^2\left(e^{-\frac{2t}{RC}}\right)}}{\mathrm{C}}. \tag{6}$$

From (6), the current across the capacitor at time t is:

$$I_C(t)=\frac{2CPe^{-\frac{2t}{RC}}-\frac{2{Q_i}^2e^{-\frac{2t}{RC}}}{RC}}{2C\sqrt{C^2PR\left(1-e^{-\frac{2t}{RC}}\right)+{Q_i}^2e^{-\frac{2t}{RC}}}}. \tag{7}$$

B. Charging time at the target node: Special case with $R\to\infty$

Target node with a RF energy harvester and an energy storage element (super-capacitor) can be modeled as a special case of constant power charging circuit shown in Fig. 2(b) with $R\to\infty$, because there is no load resistance (which represents the energy transmitter part). In this case, we obtain simpler expressions for voltage and current across the capacitor. For $R\to\infty$ in Fig. 2(b), $P=V(t)\cdot I(t)=\frac{q}{C}\cdot\frac{dq}{dt}$, which on solving for q over time 0 to t gives,

$$\int_0^Q qdq=\int_0^t PCdt \quad \text{or,} \quad Q(t)=\sqrt{2PCt}. \tag{8}$$

From (8), the voltage and current across the capacitor are respectively obtained as $V_C(t)=\sqrt{\frac{2Pt}{C}}$ and $I(t)=\sqrt{\frac{PC}{2t}}$. Also, the time T_C required to charge an uncharged capacitor up to V_C volts using constant power source with power P is:

$$T_C(C,V_C,P)=\frac{CV_C^2}{2P}. \tag{9}$$

The above equation will be used later in Section VI to determine the time required to charge the target node up to some specific voltage level for a given harvested DC power.

C. Total mean power received

With the knowledge of voltage variation during the *ON-OFF* cycle of the relay node's transmitter module, we now derive a closed-form expression for the mean power received at target node. As in most wireless power transmission and communication channels, the electromagnetic field of the transmitted RF signal is assumed to be time harmonic (sinusoidal or co-sinusoidal) with time dependence $e^{j\omega t}$, where ω is the angular frequency of the RF signal. The transmit powers of RF source and relay are P_{t_1} and P_{t_2}, respectively. The respective transmit antenna gains are $G_{t_1}(\phi_1)$ and $G_{t_2}(\phi_2)$, where ϕ_1 and ϕ_2 are standard spherical polar variables giving direction to the target receiver from respectively the RF source and relay node's transmitter on a 2-D azimuth plane with $\theta=90^\circ$. The target node receives energy from the RF source and relay with antenna gains $G_{r_T}(\phi_1)$ and $G_{r_T}(\phi_2)$ in the direction of RF source and relay node's transmitter, respectively. The relay node's receiver has the antenna gain $G_{r_r}(\phi_r)$ in the direction of RF source. The antenna gain of RF source in the direction of relay node's receiver is given as $G_{t_1}(\phi_r)$. Note that, we do not consider the elevation radiation pattern, as all the antennas are placed at the same height and the movement of relay is restricted to x-y plane only, i.e., $\theta=90^\circ$ is fixed. Also note that, $G(\phi)=G_oU(\phi)$, where G_o is the antenna gain and $U(\phi)$ is the normalized radiation (power) pattern. The mean power received at target node $\mathcal{T}$ for conjugate matched condition is:

$$\begin{aligned} \langle P_T\rangle &\triangleq P_{2HET}(x_r,y_r) \\ &= P_{r_1}+P_{r_2}(x_r,y_r)+\sqrt{P_{r_1}P_{r_2}(x_r,y_r)}\times \\ &\quad \Big\{e^{-jk(r_1-r_2(x_r,y_r))+j(\psi_1-\psi_2)}+ \\ &\quad e^{-jk(r_2(x_r,y_r)-r_1)+j(\psi_2-\psi_1)}\Big\}. \end{aligned} \tag{10}$$

Considering path loss exponent $n=2$, mean power received at the target node from the RF source is $P_{r_1}=\frac{P_{t_1}G_{t_1}(\phi_1)G_{r_T}(\phi_1)\lambda^2}{(4\pi r_1)^2}$ and that from the relay is $P_{r_2}(x_r,y_r)=\frac{D_c(x_r,y_r)P_{t_2}G_{t_2}(0^\circ)G_{r_T}(\phi_2)\lambda^2}{(4\pi r_2(x_r,y_r))^2}$. Distance between the RF source and target node is $r_1=x_0$ and that between the relay node's transmitter and target node is $r_2(x_r,y_r)=\sqrt{[x_0-(x_r+x_d)]^2+y_r^2}$, $k=\frac{2\pi}{\lambda}$, where λ is the wavelength of the RF signal, and ψ_1, ψ_2 are respectively the sum of all phases other than the path delay for RF source and relay node's transmitter. $\phi_i=\tan^{-1}\left(\frac{y_T-y_i}{x_T-x_i}\right),\forall\ i\in\{1,2\}$. It may be recalled that, $P_{DET}=P_{r_1}$ and $P_{2HET}=P_T$.

The duty cycle of relay node's transmission (defined in (2)) is given by *ON* and *OFF* state durations T_{ON} and T_{OFF}. Using (4), T_{ON} and T_{OFF} are obtained as:

$$T_{\text{ON}}(x_r,y_r)=\frac{1}{2}R_{dch}C\log\left(\frac{P_{r_r}^{DC}R_{dch}C^2-(CV_i)^2}{P_{r_r}^{DC}R_{dch}C^2-(CV_f)^2}\right) \tag{11}$$

$$T_{\text{OFF}}(x_r,y_r)=\frac{1}{2}R_{ch}C\log\left(\frac{P_{r_r}^{DC}R_{ch}C^2-(CV_i)^2}{P_{r_r}^{DC}R_{ch}C^2-(CV_f)^2}\right) \tag{12}$$

where R_{dch},R_{ch} are the resistive loads corresponding to discharging and charging modes of relay node's super-capacitor C. V_i corresponds to the minimum energy required at the relay

for its working and V_f corresponds to the fully charged super-capacitor, signifying that the relay is ready for transmission. The DC power available after rectification at the relay is:

$$P_{r_r}^{DC}(x_r, y_r) = \eta_{RFDC} P_{t_1} G_{t_1}(\phi_r) G_{r_r}(0^\circ) \left(\frac{\lambda}{4\pi r_r(x,y)}\right)^2 \tag{13}$$

where $\phi_r = \tan^{-1}\left(\frac{y_r - y_1}{x_r - x_1}\right)$ and $r_r(x_r, y_r) = \sqrt{x_r^2 + y_r^2}$ is the distance between the RF source and the relay node's receiver. η_{RFDC} is the RF-to-DC conversion efficiency, which itself is a nonlinear function of the received RF power. Note that, $\phi_1 = 0^\circ$ due to the LOS path between RF source and the target node. However, the optimal values of antenna directions ϕ_2 and ϕ_r are obtained through the ORP formulation to ensure maximum RFET gain at the target node.

We assume ψ to be normally distributed with mean$= 0$ and variance$= \overline{\psi^2}$, as phase error can be due to a number of causes and these errors are small [24]. So, (10) can be re-written as:

$$\begin{aligned} P_{2HET}(x_r, y_r) \;=\; & P_{r_1} + P_{r_2}(x_r, y_r) + \sqrt{P_{r_1} P_{r_2}(x_r, y_r)} \times \\ & 2e^{-\overline{\psi^2}} cos\left\{k\left[r_1 - r_2(x_r, y_r)\right]\right\}. \end{aligned} \tag{14}$$

IV. ORP Problem Formulation

With the expression of received power at the target node in presence of a relay at an arbitrary (non-blocking) position, we formulate an ORP problem to maximize RFET efficiency.

A. ORP on 2-D Euclidean plane

From (10), it is clear that simultaneous reception from RF source and relay node can only be beneficial if the arriving RF waves at the target node are aligned in phase. The RF waves combine at the target node constructively or destructively depending upon the relative path or phase differences between the energy transmitters and the target node. Specifically, when the relay node is placed at such a position that leads to a path difference of integral multiple of the signal wavelength λ, it gives rise to constructive interference. As $y = y_0$ is the closest distance from the LOS path, intuitively it appears that the relay node can be placed at this distance away from LOS path and then moved along *x-axis* to find optimal position. However it may not be the right choice because a particular $(x_r, y_r = y_0)$ position may cause destructive interference at the target node. In order to combat or overcome the destructive interference at every *x-axis* position, the distance along *y-axis* is extended from y_0 up to a point where the path difference is $\frac{\lambda}{2}$, as this range covers all the phase difference possibilities from 0 to π for a given x-axis position. Optimal position of the relay node is determined with respect to its receiver's position (x_r, y_r) to maximize the received power at the target node. Noting that, the relay node's transmitter is separated by a distance x_d from its receiver, the optimization problem can be formulated as:

$$\begin{aligned} (P0): \quad \max_{x_r, y_r} \quad & \langle P_T \rangle = P_{2HET}(x_r, y_r) \\ \text{s.t.} \quad & C1: 0 \le x_r \le x_0 - x_d \\ & C2: y_0 \le y_r \le y_u(x_r) \end{aligned} \tag{15}$$

where $P_{2HET}(x_r, y_r)$ is defined in (14) and $y_u(x_r) = \sqrt{\left(\frac{\lambda}{2}\right)^2 + y_0^2 + \lambda\sqrt{x_0 - (x_r - x_d)^2 + y_0^2}}$.

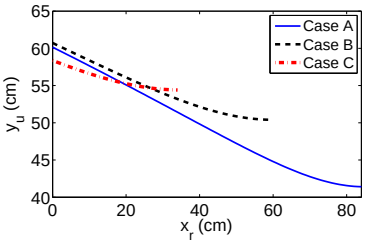

Fig. 3: y_u variation with x_r.

As, the upper bound y_u on y_r, is a decreasing function of x_r, as shown in Fig. 3 (for the 3 cases as defined later in Section VI), $y_u(x_r)$ can be replaced by $y_u(0)$ in $C2$ in order to have linear box constraints. So, the modified optimization problem with updated box constraint $C2$ is:

$$\begin{aligned} (P1): \quad \max_{x_r, y_r} \quad & P_{2HET}(x_r, y_r) \\ \text{s.t.} \quad & C1: 0 \le x_r \le x_0 - x_d \\ & C2: y_0 \le y_r \le y_u(0). \end{aligned} \tag{15a}$$

It should be noted that the solution of $P1$ in (15a) is always better than the problem $P0$ in (15), because the feasible region of $P0$ is a proper subset of the feasible region of $P1$. The problem in (15a) is nonconvex because the objective function to be maximized is nonconcave. The problem is also highly nonlinear because of involvement of the terms D_c, P_{r_2}, and $cos\left\{k\left(r_1 - r_2\right)\right\}$ – which are nonlinear composite functions of relay node's position (x_r, y_r).

B. ORP with distributed beamforming

Since the RF source and relay node's transmission do not effect each other, we can use distributed beamforming for increasing the η_E. Also, since the position of the RF source is known and relay has to be placed on the feasible Euclidean x-y plane defined by the constraints C1 and C2 in (15a), their local oscillators can be synchronized in a manner that a controlled phase shift can be introduced to compensate for the path or range differences, thereby realizing a constructive interference at the target node. In this way, instead of moving along the y-axis to get in-phase energy waves at the target node for a given x-axis position, the relay node is simply moved along the x-axis at y_0 distance from LOS path. This reduces the ORP problem defined in (15a) to a single-dimensional (or one variable) nonconvex problem $P2$, given below:

$$\begin{aligned} (P2): \max_{x_r} P_{2HET}^{DB} &= P_{r_1} + P_{r_2}(x_r, y_0) + 2\sqrt{P_{r_1} P_{r_2}(x_r, y_0)} \\ \text{s.t.} \quad & C1: 0 \le x_r \le x_0 - x_d. \end{aligned} \tag{16}$$

Here, the phase difference and path difference related terms are removed from the formulation (15a), because the controlled phase differences cancel out the underlying path difference between the energy waves reaching at the target from the RF source and the relay.

It is clear from the formulations in (15a) and (16) that, $P2$ can provide a higher RFET efficiency because, relay's movement only along the x-axis at y_0 distance from the LOS path reduces the RF source-to-relay-to-destination distance.

C. Constructive and destructive interference regions

From (14), it can be seen that the cosine term in received power $P_{2HET}(x_r, y_r)$ decides whether the underlying relay position leads to constructive or destructive interference of the received signal power P_{r_1} from the RF source and $P_{r_2}(x_r, y_r)$ from the relay. If the cosine term is negative, it leads to destructive interference. In other words, mathematically, since $2e^{-\overline{\psi^2}}\sqrt{P_{r_1}P_{r_2}(x_r,y_r)} > 0$, if $\cos(\cdot) < 0$ in (14), $P_{2HET}(x_r, y_r) < P_{r_1} + P_{r_2}(x_r, y_r)$. But the major concern is when due to this destructive interference, the received power in 2HET is even lower than the DET. This is critical because the relay placed at such positions performs adversely, and it makes ORP even more significant in 2HET. At such positions, defined below by set $\mathcal{D}_{\mathcal{I}}$, RFET efficiency provided by DET is superior to that of 2HET, i.e.,

$$\begin{aligned}\mathcal{D}_{\mathcal{I}} &= \{(x_r, y_r) \mid P_{2HET}(x_r, y_r) < P_{DET}\} \\ &= \{(x_r, y_r) \mid P_{r_2}(x_r, y_r) + P_{r_{12}}(x_r, y_r) < 0\} \quad (17)\end{aligned}$$

where $P_{r_{12}}(x_r, y_r)$ is given as:
$P_{r_{12}}(x_r, y_r) = 2\sqrt{P_{r_1}P_{r_2}(x_r, y_r)}e^{-\overline{\psi^2}} cos\{k[r_1 - r_2(x_r, y_r)]\}$.
Similarly, the set $\mathcal{C}_{\mathcal{I}}$ defines the region of constructive interference, where the relay position is such that 2HET provides RFET efficiency improvement over DET, i.e.,

$$\mathcal{C}_{\mathcal{I}} = \{(x_r, y_r) \mid P_{2HET}(x_r, y_r) \geq P_{DET}\}. \quad (18)$$

Fig. 4(a) plots the regions of relay node position causing constructive or destructive interference. From the above discussion

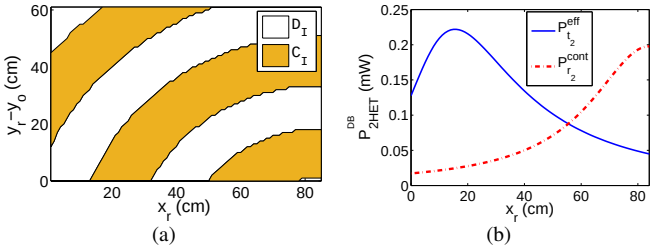

Fig. 4: Numerical ORP characteristics (Powercast P1110 harvester system; end-to-end distance $x_0 = 100$ cm). (a) Constructive and destructive interference regions against relay position in 2HET without beamforming. (b) Tradeoff in 2HET with distributed beamforming.

and (16) it can be noted that, ORP with distributed beamforming does not suffer from the destructive interference problem, i.e., at all relay positions $P^{DB}_{2HET}(x_r) > P_{DET}, \forall\, x_r$, because in this case $P^{DB}_{r_{12}}(x_r) = P_{r_2}(x_r, y_0) + 2\sqrt{P_{r_1}P_{r_2}(x_r, y_0)} > 0, \forall\, x_r$. This is another advantage of distributed beamforming case $(P2)$ over the 2-D Euclidean case $(P1)$.

D. Tradeoff at the relay: Scavenged versus delivered energy

From (15a) and (16), it is clear that the mean received power at target node P_{2HET} (or P^{DB}_{2HET}) is composed of two power terms P_{r_1} and P_{r_2}, where P_{r_1} is constant and P_{r_2} is a function of relay node's position (x_r, y_r). Unlike in $P1$, where apart from optimizing P_{r_2}, destructive interference also needs to be tackled, in $P2$ only P_{r_2} is needed to be optimized. In this subsection we discuss the tradeoff that exists while deciding the ORP for maximizing P_{r_2} which in turn maximizes P^{DB}_{2HET}.

As the relay node transmits the RF energy harvested from transmission of the RF source to the target node, closer to the RF source may be a better position to harvest a higher amount of energy. A higher mean harvested energy at relay node $P^{DC}_{r_r}$ implies a higher duty cycle D_c. This in turn implies a higher effective transmit power from the relay node, given as:

$$P^{\text{eff}}_{t_2}(x_r, y_r) = D_c(x_r, y_r)P_{t_2}. \quad (19)$$

However, if harvesting part is neglected and relay is assumed capable of continuous transmission at P_{t_2}, then to maximize the received power P_{r_2}, path loss has to be minimized. In this scenario, a position closer to the target node is more suited as it suffers from lesser path loss. Received power at the target node due to this continuous transmission of relay is:

$$P^{\text{cont}}_{r_2}(x_r, y_r) = \frac{P_{t_2}G_{t_2}(0°)G_{r_T}(\phi_2)\lambda^2}{(4\pi r_2(x_r, y_r))^2}. \quad (20)$$

So, basically $P2$ solves this nontrivial tradeoff between energy scavenged and effective energy delivered. An example case is shown in Fig. 4(b) (more will be discussed in Section VI).

V. Global Optimization Algorithm

In general there exists no standard approach for finding the global optimal solution for the nonconvex optimization problems. In many cases, determining the exact global optimal solution is either computationally very expensive or not possible in finite amount of time. So we try to find the global optimum within some acceptable tolerance $\epsilon > 0$ [25]. In particular, we find ϵ-global maximum, which is defined below.

Definition 1: If $x^* \in \mathcal{F}$ is a feasible solution with some acceptable tolerance $\epsilon > 0$, where $\mathcal{F}$ is a non-empty convex set in $\mathbb{R}^n$ and $f(x) \leq f(x^*) + \epsilon, \quad \forall x \in \mathcal{F}$, then x^* is an ϵ-global maximum.

A global optimization algorithm based on branch and bound (BB) method was proposed in [26]. Convex lower bounding function $\mathcal{L}$ was used along with efficient partitioning strategy to achieve guaranteed convergence to the ϵ-global optimum solution for nonlinear, twice differentiable nonconvex functions. The basic idea is to first partition the feasible set into smaller subsets (following the *divide and conquer* strategy), then find lower and upper bounds of the underlying optimization problem (minimization) respectively by solving the convex lower bounding function $\mathcal{L}$ and finding the actual objective function value at that point. This results in a non-decreasing sequence for the lower bound, as $\mathcal{L}$ is solved over a smaller feasible region with increasing number of iterations and a non-increasing sequence for the upper bound as the infimum over all the previously recorded upper bounds is stored in it. If the global minimum obtained by solving $\mathcal{L}$ over a feasible subset is greater than the current upper bound, then this subset is not considered further (*fathoming* step). At each step, the global lower and upper bounds are updated and if they are close enough, the process is ended. Otherwise the partition with tighter constraints is selected and the process is repeated.

This BB method works very well in our case because our objective function is twice differentiable with box-constraints. Moreover, the convergence to ϵ-global optimal is faster as there

are only a few modes (a few local minima) which actually depends on the distance x_0 between RF source and target node. Let (x_r^*, y_r^*) be the ORP and P_{2HET}^* be the maximum received power at the target node. The convex lower bounding function is defined for minimization function, so we minimize the negative of the objective function defined in (15a) and (16). The convex lower bounding function $\mathcal{L}$ for $-P1$ is given by:

$$\begin{aligned}\mathcal{L}(x_r, y_r) \;=\; & -P_{2HET}(x_r, y_r) + \alpha\left\{[0 - x_r]\,[x_0 - x_d - x_r]\right. \\ & \left. + \,[y_0 - y_r]\,[y_u(x_r) - y_r]\right\}. \end{aligned} \tag{21}$$

Here parameter α should satisfy the constraint [26]:

$\alpha \geq \max\left\{0, \max\limits_{\substack{i \\ x_i^L \leq x_i \leq x_i^U}} \left(-\frac{1}{2}\lambda_i^{P_{2HET}}\right)\right\}$, where $\lambda_i^{P_{2HET}}$ are the eigenvalues of the Hessian matrix of the function P_{2HET} and $x_i \in \{x_r, y_r\}$. In [21], [25], several methods for estimating the appropriate value of parameter α were given. In our case there are only two variables, so we find an approximate lower bound for α by finding the minimum eigenvalue from the set of eigenvalues of the Hessian matrix which is a function relay position (x_r, y_r), for the cases when $(x_r, y_r) \in \mathbb{Z}$ (set of integers). This is not very computationally expensive as the feasible region is not very large. Accordingly, in our case $\mathcal{L}$ as defined in (21) is actually a near convex function (NCF).

We use Conjugate Gradient Method (CGM) with positive Polak-Ribiere (PR) beta [27], to solve convex relaxation $\mathcal{L}$ problem globally and the original problem ($-P1$ or $-P2$) locally at each iteration. This iterative algorithm provides very good convergence, and also due to the presence of highly nonlinear terms in the objective function it is not possible to obtain the explicit analytic solution. Also, we use Golden-section based line search [28] technique within the upper and lower bounds such that the feasibility constraints are met.

We have slightly modified the αBB algorithm, by finding the upper bound on $-P_{2HET}^*$ by solving $-P1$, rather than by simply calculating $-P_{2HET}$ at the global minimum point of $\mathcal{L}$. This provides faster convergence by finding tighter upper bound at each iteration and thus reducing the number of sub-search spaces. The proposed algorithm is summarized in Algorithm 1. Algorithm 1 terminates when either the maximum of iteration I_{max} is reached, or when the ϵ-global optimum solution is found, i.e., the normalized gap $\left(\frac{P_{2HET}^U - P_{2HET}^L}{P_{r_1}}\right) < \xi$, where P_{2HET}^U and P_{2HET}^L are the upper and lower bounds on $-P_{2HET}^*$. Generally, $\epsilon = 10^{-3}$ is considered to be acceptable value, but ideally value of ϵ should decided based upon the approximate value of the global optimum. As in our proposed ORP problem, the optimal received power is in the range of received single hop power P_{r_1}, so $\epsilon = \xi P_{r_1}$. It may be recalled that the Algorithm 1 solves a minimization problem. However, as ours is a maximization problem, we solve for $-P1$.

Algorithm 1 can also be used for beamforming-based formulation $P2$, but with a few modifications. As $P2$ reduces to one dimension only, the search for minimum and splitting occurs only along *x-axis* (*y-axis* position is fixed to y_0) and as a result $\mathcal{L}$ and α are calculated using P_{2HET}^{DB} and the boundary constraints on x_r. Algorithm 1 converges very fast for $P2$.

Algorithm 1 Proposed modified αBB algorithm.

Input: x_0, y_0, x_d, I_{max} and ξ
Output: P_{2HET}^*, x_r^*, y_r^*

1: Initialize upper and lower bounds on x and y as $x_1^U = x_0 - x_d$, $x_1^L = 0$, $y_1^U = y_u(0)$, $y_1^L = y_0$. Set $i = 0$. Find P_{r_1} and set $\epsilon = \xi P_{r_1}$.
2: Run *CGM* algorithm to solve $-P1$ (nonconvex) in the entire feasible region and obtain a local minimum solution $\left(x_{0,r}^*, y_{0,r}^*\right)$ with function value P_{2HET}^U (initial upper-bound)
3: Find parameter α as:

$$\alpha = \max\left\{0, \max_{\substack{j \\ z_{j1}^L \leq z_j \leq z_{j1}^U}} \left(-\frac{1}{2}\lambda_j^{P_{2HET}}\right)\right\} \tag{22}$$

where $\lambda_j^{P_{2HET}}$ are the eigenvalues of the Hessian matrix of the function P_{2HET}, $z_j \in \{x, y\}$ and $(x, y) \in \mathbb{Z}$. Solve the convex relaxation $\mathcal{L}$ of $-P1$ using *CGM* algorithm in the entire feasible region to obtain initial lower-bound P_{2HET}^L.
4: **if** $\left(P_{2HET}^U - P_{2HET}^L\right) > \epsilon$ **then** set $i = 1$.
5: **else** $P_{2HET}^* = -P_{2HET}^U$, $x_r^* = x_{0,r}^*$, $y_r^* = y_{0,r}^*$, **break**
6: **repeat** (Main Loop)
7: Split $\left\{(x, y) \;\middle|\; x_i^L \leq x \leq x_i^U \wedge y_i^L \leq y \leq y_i^U\right\}$ (current region) into two subregions ($s = 1$ or left and $s = 2$ or right) along its longer edge given by $\max\left\{\left(\frac{x_i^U - x_i^L}{x_0 - x_d}\right), \left(\frac{y_i^U - y_i^L}{y_u(x_i^L) - y_0}\right)\right\}$. Store the upper and lower bounds on x and y in these two regions in $x_{i,s}^U, y_{i,s}^U, x_{i,s}^L, y_{i,s}^L$. Apply *CGM* to both the regions to find the global optimum by solving $\mathcal{L}$ in the shrinked regions:

$$\begin{aligned}\mathcal{L}(x_r, y_r) = \quad & -P_{2HET}(x_r, y_r) + \alpha\left\{\left[x_{i,s}^L - x_r\right]\right. \\ & \left.\left[x_{i,s}^U - x_r\right] + \left[y_{i,s}^L - y_r\right]\left[y_{i,s}^U - y_r\right]\right\}\end{aligned}$$

where, α is as obtained as defined in (22), but in the region defined by $\left\{(x, y) \;\middle|\; x_{i,s}^L \leq x \leq x_{i,s}^U \wedge y_{i,s}^L \leq y \leq y_{i,s}^U\right\}$. Store the global minimum solutions in $P_{2HET}^{L_{i,s}}$.
8: **if** $(P_{2HET}^{L_{i,s}} \leq P_{2HET}^U)$ **then** solve $-P1$ in these regions to find local optimum solution with solution points and store them in $P_{2HET}^{U_{i,s}}$, $(x_{i,s}, y_{i,s})$, respectively.
9: **else** delete the $P_{2HET}^{L_{i,s}}$ from the stored result.
10: **if** $\mid P_{2HET}^{L_{i,s}} \mid = 0$ i.e., all subsets fathomed **then break**
11: Set $i = i + 1$
12: Set $P_{2HET}^L = \min\limits_{I,s} P_{2HET}^{L_{I,s}}, \quad I = 1, .., i-1 \qquad s = 1, 2$
13: Set $i^*, s^* = \operatorname{argmin}\limits_{I,s} P_{2HET}^{L_{I,s}}, \quad I = 1, .., i-1 \qquad s = 1, 2$
14: Set $x_i^L = x_{i^*,s^*}^L$, $x_i^U = x_{i^*,s^*}^U$, $y_i^L = y_{i^*,s^*}^L$, $y_i^U = y_{i^*,s^*}^U$
15: New region: $\left\{(x, y) \;\middle|\; x_i^L \leq x \leq x_i^U \wedge y_i^L \leq y \leq y_i^U\right\}$
16: **if** $P_{2HET}^U \geq P_{2HET}^{U_{i^*,s^*}}$ **then**
17: $P_{2HET}^U = P_{2HET}^{U_{i^*,s^*}}$
18: $P_{2HET}^* = -P_{2HET}^U$, $x_r^* = x_{i^*,s^*}$, $y_r^* = y_{i^*,s^*}$
19: Delete all the results corresponding to i^*, s^*
20: **until** $\left(P_{2HET}^U - P_{2HET}^L\right) \leq \epsilon$ or $i = I_{max}$

A. Faster convergence of the proposed algorithm

The feasible region of ORP is given as, $\mathcal{F}_{\mathcal{R}} = \{(x_r, y_r) \mid 0 \leq x_r \leq x_0 - x_d \wedge y_0 \leq y_r \leq y_u(0)\}$. The diagonal of $\mathcal{F}_{\mathcal{R}}$ or the subset of $\mathcal{F}_{\mathcal{R}}$ during iteration i as a function of the box constraint ($x_r \in \left[x_i^L, x_i^U\right]$ and $y_r \in \left[y_i^L, y_i^U\right]$) is:

$$D_i = \sqrt{\left(x_i^U - x_i^L\right)^2 + \left(y_i^U - y_i^L\right)^2}. \tag{23}$$

When $D_i < \delta = \sqrt{\frac{4\epsilon}{\alpha}}$, the ϵ-global optimum is achieved. The longest diagonal corresponding to the initial complete feasible rectangular region is:

$$D_0 = \sqrt{(x_0 - x_d)^2 + (y_u(0) - y_0)^2}. \tag{24}$$

Then, the upper bound I^U and lower bound I^L on the maximum number of number of iterations required for convergence to ϵ-global minimum of $-P1$ and $-P2$ are:

$$I^U = \begin{cases} \left\lceil \left(\frac{D_0}{\delta}\right)^2 - 1 \right\rceil, & \text{for } P1 \\ \left\lceil \frac{x_0 - x_d}{\delta} - 1 \right\rceil, & \text{for } P2 \end{cases} \tag{25}$$

$$I^L = \begin{cases} \left\lceil 2\log_2\left(\frac{D_0}{\delta}\right) - 1 \right\rceil, & \text{for } P1 \\ \left\lceil \log_2\left(\frac{x_0 - x_d}{\delta}\right) - 1 \right\rceil, & \text{for } P2. \end{cases} \tag{26}$$

The reasons for faster convergence of the algorithm are:

1) Low dimensionality of the ORP problem: The dimension of the proposed ORP $P1$ and $P2$ in (15a) and (16) is two and one, respectively. Due this low dimensionality there are only two summation terms in the numerator of (25) and (26) for $P1$ and only one term for for $P2$. This leads to lower values of I^U and I^L for the termination of the Algorithm 1.

2) Smaller range of RFET: The range of RFET is limited due to the limits on maximum transmit power, path loss, low receiver sensitivity and low RF to DC conversion efficiency at very low input RF power. For example in commercially available RF energy harvesting module from Powercast P1110, rectification efficiency is below 10% at input RF power received below -5 dBm [22]. This limits the range of RFET, because if the received RF power is below -5 dBm, effectively there is no RF energy harvesting. Due to this RFET range is smaller (on the order of a few meters only), the values of $(x_0 - x_d)^2$ and $(y_u(0) - y_0)^2$ (box constraints) are low, which in turn results in lower value of I^U and I^L.

3) Very low value of α: As α is determined using the Hessian matrix values over the discrete positions in the feasible region, we are able to obtain a tighter lower bound on α. These values of α, discussed in Section VI, are very low, resulting in low value of I^U and I^L because, as $\alpha \to 0, \delta \to \infty$.

Apart from these reasons, in practice the total number of iterations required for termination is much closer to I^L rather than to I^U, as shown in next section via numerical results.

VI. Numerical Results

In this section we evaluate the performance of the proposed algorithm in solving nonconvex optimization problems $P1$ and $P2$ with commercial RF energy harvester from Powercast P1110 [22] as an example. We have considered three feasible region cases as mentioned in Table I. The distances beyond 100 cm have not been considered due to low RFET range. Other system parameters considered are given in Table II.

TABLE I: Three cases considered.

Case	RF source to target node distance x_0 (cm)	Minimum non-blocking distance of relay from LOS path y_0 (cm)	Upper bound on y_r $y_u(0)$ (cm)
A	100	25	60.15
B	75	34	60.72
C	50	38	58.37

TABLE II: System parameters.

S.No.	System parameter	Symbol	Value
RF source (Agilent RF synthesizer N9310A) + Powercast 915 MHz PCB patch (directional) antenna			
1	Transmit power	P_{t_1}	20 dBm
2	Antenna gain	G_{t_1}	6.1 dBi
3	Power consumption	P_{cons}	74.17 W
Relay node (Powercast P1110 evaluation board + modified Mica2 mote + two Powercast 915 MHz PCB patch (directional) antennas)			
4	Transmit power	P_{t_2}	5 dBm
5	Receive antenna gain	G_{r_r}	6.1 dBi
6	Transmit antenna gain	G_{t_2}	6.1 dBi
7	Super-capacitor	C	50 mF
8	Final voltage level	V_f	3 V
9	Initial voltage level	V_i	2 V
10	Charging load resistance	R_{ch}	100 Ω
11	Discharging load resistance	R_{dch}	375 kΩ
Target node (Powercast P1110 evaluation board + Powercast 915 MHz PCB dipole (omnidirectional) antenna)			
12	Receive antenna gain	G_{r_T}	1 dBi
13	Super-capacitor	C	50 mF
14	Final voltage level	V_f	3 V
Algorithm 1			
15	Iteration bound	I_{max}	100
16	Normalized tolerance	ξ	0.001
Miscellaneous			
17	Operating frequency	f	915 MHz
18	Root mean square (RMS) phase error	$\overline{\psi^2}$	10°
19	Distance between receiver and transmitter antenna at the relay	x_d	16 cm
20	Path loss exponent	n	2

Powercast 915 MHz PCB patch and dipole antennas were used and their radiation patterns in azimuth plane ($\theta = 90°$) was found out by performing measurements in the RF anechoic chamber. Fig. 5(a) shows that the measured normalized radiation pattern of the patch antenna can be very closely approximated by a 10-degree polynomial fit [29] given as:

$$\begin{aligned} U(\phi) = &-0.00001\phi^{10} + 0.00021\phi^9 - 0.002214\phi^8 + 0.01043\phi^7 \\ &-0.01139\phi^6 - 0.07684\phi^5 + 0.23374\phi^4 + 0.06288\phi^3 \\ &-0.76824\phi^2 + 0.12571\phi + 0.99803. \end{aligned}$$

The norm of residuals for poly-fitting is 0.0114, which is within acceptable limit of allowable model-fitting errors [30].

Relay node's receiver part harvests the RF power received from the RF source via 6.1dBi directional antenna, converts it to DC and stores it in a 50 mF super-capacitor. The RF to DC efficiency of the P1110 IC is a function of the input RF power [22] and is plotted in Fig. 5(b) along with the 20-degree polynomial fit curve which very closely approximates this behavior. Relay node's transmitter part includes a modified Mica2 mote which is powered from the energy stored in 50mF super-capacitor and transmits energy at $+5$ dBm, in the form of data packets via 6.1 dBi antenna to the target node. For efficient RFET, Mica2 has been programmed to transmit dummy data packets continuously one after the another during the *ON* state [5]. We experimentally found that Mica2 mote consumes 8 μA and 30 mA at 3 V during *OFF* and *ON* state, which translates to $R_{dch} = 0.375$ MΩ and $R_{ch} = 100$ Ω resistive loads, respectively. The voltage corresponding to the minimum energy threshold and fully charged super-capacitor are $V_i = 2$ V and $V_f = 3$ V, respectively. Based on this and the *ON-OFF* model for relay node, as discussed in Section III, we have plotted the super-capacitor's voltage $V_C(t)$ variation

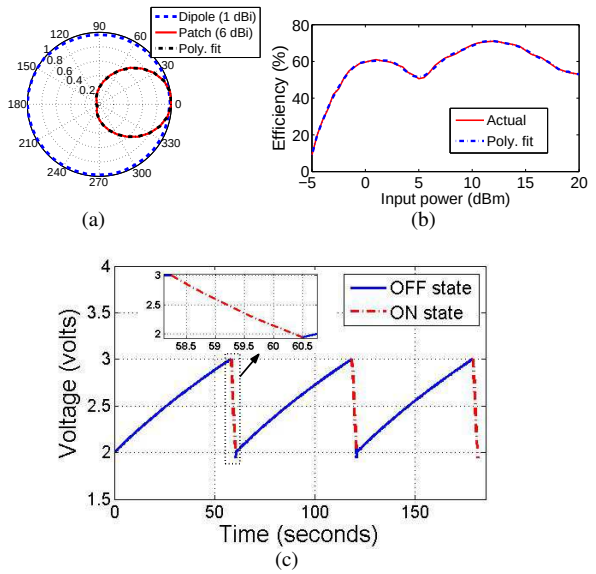

Fig. 5: (a) Normalized radiation (power) plot in azimuth plane. (b) Powercast P1110 RF to DC efficiency variation with input RF power. (c) Duty cycle of relay's transmitter at optimal position for case C.

with time in Fig. 5(c) based on the duty cycle D_c obtained numerically for the ORP in 2-D problem $P1$.

After experimentally estimating the system parameters, listed in Table II, we present the numerical results using the proposed analytical model, mathematical equations derived, and the theoretical results obtained from Algorithm 1.

A. Received mean power P_{2HET} variation with relay position

Fig. 6(a), 7(a), and 8(a) shows the variation of the mean power received P_{2HET} at target node in the 2-D feasible region (problem $P1$) for case A, case B, and case C, respectively. It shows that objective function is nonconcave. It also indicates that the number of modes and complexity of $P1$ increases with increasing RF source to target node distance x_0.

Fig. 6(b), 7(b), and 8(b) shows the variation of the mean power received P^{DB}_{2HET} at the target node using distributed beamforming in the 1-D feasible region (problem $P2$) for case A, case B, and case C. It also shows that the complexity of the problem increases with increasing x_0. As this problem is far more simpler than the 2-D problem $P1$, we have also shown the step by step working of the Algorithm 1 for $P2$ in Fig. 6(b), 7(b), and 8(b). For case C, the first local solution of $P2$ itself is the ϵ-global optimal solution, so no more iterations of the Algorithm 1 are required. Whereas in case A and case B, it takes two and one iterations, respectively, to find the ϵ-global optimal solution. After first iteration in case A, as the lower bound provided by solving $\mathcal{L}$ in right partition of x-axis, i.e. NCF 1 Right, is lower than the one found by solving in left partition, i.e. NCF 1 Left, so in second iteration, NCF 1 Right becomes the new feasible region to be split. Fig. 6(b) shows that for case A, NCF $\mathcal{L}$ of the right side partition in second iteration, i.e. NCF 2 Right, very closely approximates the actual function, such that the difference between the local minimum of actual problem $P2$ in this range and the global minimum of NCF 2 Right are within the acceptable tolerance ϵ, so the algorithm terminates. Similarly, Fig. 7(b) shows that for case B, NCF of the right side partition in first iteration, i.e. NCF 1 Right, very closely approximates the actual function, such that the solution found is ϵ-global maximum.

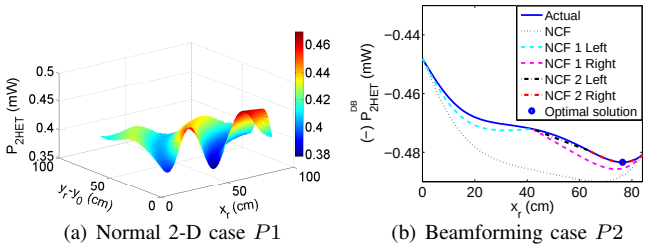

(a) Normal 2-D case $P1$ (b) Beamforming case $P2$

Fig. 6: Received mean power plot for case A.

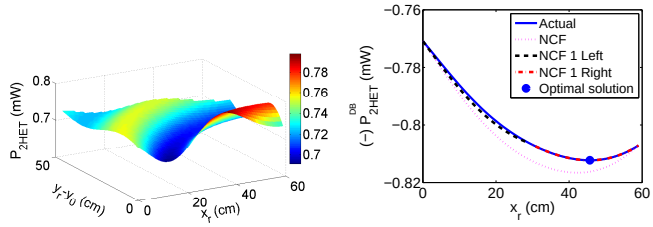

(a) Normal 2-D case $P1$ (b) Beamforming case $P2$

Fig. 7: Received mean power plot for case B.

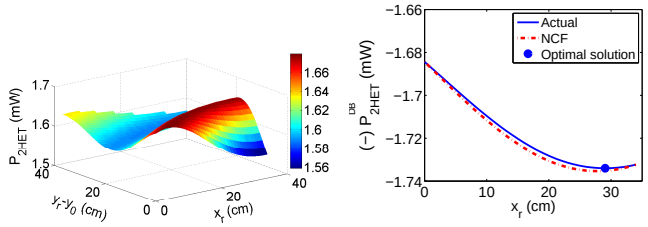

(a) Normal 2-D case $P1$ (b) Beamforming case $P2$

Fig. 8: Received mean power plot for case C.

B. Convergence of the proposed algorithm

The convergence of the global optimization algorithm – Algorithm 1 for ORP in 2-D space (problem $P1$) is shown in Fig. 9 which plots the evolution of upper bound P^U_{2HET} and lower bound P^L_{2HET} to the optimal value of $-P1$ with increasing iterations for case A, case B, and case C. The results show that because of the modifications in the conventional α-based BB method and low dimensionality of the optimization problem, Algorithm 1 converges to ϵ-optimal solution in few iterations I_{iter} only. Also, it has to be noted that convergence is faster in the beginning as the gap between the upper and lower bound reduces very sharply in the initial few iterations.

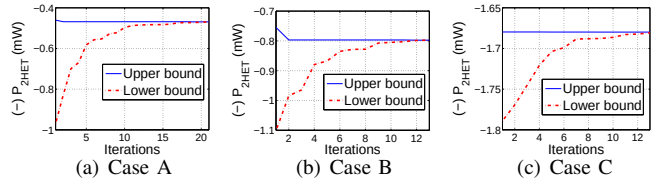

Fig. 9: Illustration of the convergence of Algorithm 1 for $P1$.

TABLE III: Convergence results.

Case		ϵ	α	D_0	δ	I^U	I^L	I_{iter}	
								Original αBB [21]	Proposed Algorithm 1
A	P1	1.62×10^{-6}	8.09×10^{-7}	91.06	1.44	4004	11	23	21
	P2		7.91×10^{-9}	84	14.55	5	2	2	2
B	P1	7.34×10^{-7}	9.61×10^{-7}	64.77	1.75	1372	10	14	13
	P2		6.53×10^{-9}	59	21.21	2	1	1	1
C	P1	4.19×10^{-7}	7.79×10^{-7}	39.64	2.88	188	7	14	13
	P2		8.50×10^{-9}	34	27.61	1	0	0	0

Table III shows the convergence results of the proposed algorithm for the 3 cases of both $P1$ and $P2$. It is clear that the actual number of iterations I_{iter} is very close to the lower bound I^L and very less as compared to the upper bound I^U. The value of α is very low, which leads to a high value of δ, that ultimately leads to fast convergence as shown in the table. Also $\alpha > 0$ in each case implies that both $P1$ and $P2$ are nonconvex, as their objective functions are nonconcave.

We have also compared the performance of the proposed Algorithm 1 (modified αBB) with the original αBB method [21] in terms of number of iterations I_{iter} required for convergence. The results show that the proposed Algorithm 1 provides about 9% faster convergence in $P1$. Note that there is no tangible improvement with modified αBB in case of $P2$, which is because of pseudo-concavity of its objective function.

C. Pseudoconcavity of ORP with distributed beamforming $P2$

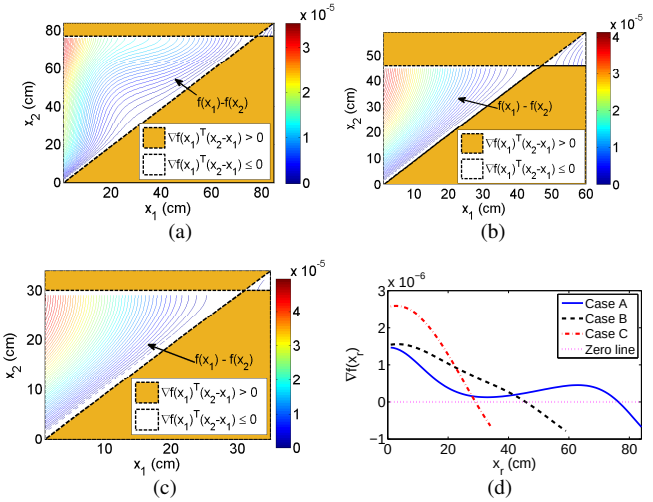

Fig. 10: Graphical explanation of pseudoconcavity of ORP problem for distributed beamforming case $P2$. (a), (b), and (c) show that $\forall\ x_1, x_2 \in \mathcal{F}$ (where $\mathcal{F}$ is the feasible region), $\nabla f(x_1)^\intercal (x_2 - x_1) \leq 0 \implies f(x_1) - f(x_2) \geq 0$, for the cases A, B, and C, respectively. (d) Gradient (first derivative) of the objective function of $P2$.

ORP with distributed beamforming (problem $P2$) with Powercast P1110 energy harvester and antenna turns out to be pseudoconcave. That is, $\forall\ x_1, x_2 \in \mathcal{F}$ (where $\mathcal{F}$ is the convex feasible region defined in the closed interval $[0, x_0 - x_d]$), $\nabla f(x_1)^\intercal (x_2 - x_1) \leq 0 \implies f(x_1) - f(x_2) \geq 0$, where f is the objective function of the optimization problem $P2$ in (16). The pseudoconcavity of $P2$ is shown graphically in Figs. 10(a), (b), and (c) for the cases A, B, and C. The entire convex feasible region $\mathcal{F}$ is divided into 2 regions: $\mathcal{F}_\mathcal{A} = \{(x_1, x_2) \mid \nabla f(x_1)^\intercal (x_2 - x_1) \leq 0\}$ and $\mathcal{F}_\mathcal{B} = \{(x_1, x_2) \mid \nabla f(x_1)^\intercal (x_2 - x_1) > 0\}$. The results in Fig. 10(a), (b), and (c), illustrate that $f(x_1) - f(x_2) \geq 0, \forall\ (x_1, x_2) \in \mathcal{F}_\mathcal{A}$. This implies that P^{DB}_{2HET} is a pseudoconcave function of x_r.

Pseudoconcavity of P^{DB}_{2HET} has also been explained with the help of Fig. 10(d), which shows that if, $\exists\ \hat{x}$ such that $\nabla f(\hat{x}) = 0$, then $\hat{x}$ is a global maximum [31]. Due to this property, the first local solution obtained in the first step by the CGM algorithm, where the gradient vanishes, is itself the global optimum (or ϵ-global maximum) solution, i.e. no additional iteration of the proposed global optimization is required. One and two iterations that required for case B and A, respectively, are actually required to obtain a tighter lower bound such that the difference between the local solution of $-P2$ and corresponding lower bound is within ϵ.

D. RFET efficiency improvement

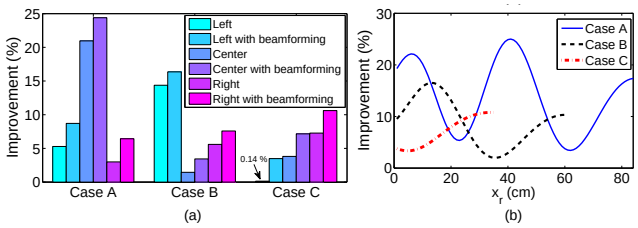

Fig. 11: (a) 2HET efficiency improvement with ORP over 2HET with arbitrary relay positions (e.g., left, center, right). (b) 2HET efficiency improvement with distributed beamforming over normal 2HET.

Fig. 11(a) shows that, 2HET with ORP increases RFET performance (η_E) with respect to 2HET with arbitrarily-placed relay (e.g., left ($x_r = \frac{x_0}{4} - \frac{x_d}{2}, y_r = y_0$), center ($x_r = \frac{x_0}{2} - \frac{x_d}{2}, y_r = y_0$), or right ($x_r = \frac{3x_0}{4} - \frac{x_d}{2}, y_r = y_0$) [1], [5]). Also, 2HET with ORP and distributed beamforming shows consistently higher performance over normal 2HET with ORP. This improvement in η_E achieved through ORP via $P1$ with $y_r = y_0$ against the arbitrary relay positions, is:

$$\Delta\eta_E(x_r) = \eta^*_E - \eta_E(x_r) = \left(\frac{P^*_{2HET} - P_{2HET}(x_r, y_0)}{P_{DET}}\right) \times 100$$

where $\eta^*_E = \left(\frac{P^*_{2HET} - P_{DET}}{P_{DET}}\right) \times 100$. Similarly the improvement in 2HET with distributed beamforming $P2$ and ORP is given as:

$$\Delta\eta^{DB}_E(x_r) = \eta^{DB^*}_E - \eta_E(x_r) = \left(\frac{P^{DB^*}_{2HET} - P_{2HET}(x_r, y_0)}{P_{DET}}\right) \times 100$$

where $\eta^{DB^*}_E = \left(\frac{P^{DB^*}_{2HET} - P_{DET}}{P_{DET}}\right) \times 100$ and $P^{DB^*}_{2HET}$ is the received power at target node in ORP with distributed beamforming. The trends of improvement with ORP is however not monotonic; instead it is a function of source-destination distance x_0. For example, at $x_0 = 100$ cm (case A), the highest gain of ORP+beamforming (25%) is with respect to center-positioned relay. In cases B and C, the highest gains (15% and 10%) occur respectively with respect to the left and right positioned relay.

Fig. 11(b) depicts the oscillatory behavior of RFET gain improvement provided by 2HET with beamforming ($P2$) against normal 2HET ($P1$) with $y_r = y_0$, which is clearly due to constructive and destructive interference associated with $P1$. The plots here reiterate that, the maximum gains with different x_0 values occur at different ORP distance x_r.

Thus, *distributed beamforming offers simplicity in relay placement as well as more gain, however at the cost of added synchronization requirement at the RF source and relay node.*

E. Energy savings provided by ORP

RFET efficiency improvement eventually leads to energy savings of the RF source. However, due to nonlinear dependence of RFET efficiency improvement and energy savings achieved at the RF source, they do not have a constant scaling based relationship. So here we derive the energy saving expression and present the corresponding numerical results.

Agilent RF synthesizer N9310A was used as the RF source consumes power during RFET to the target node. The measured power consumption $P_{cons} = 74.17$ W of this RF source transmitting at $+20$ dBm was used in the numerical model. Energy saving with ORP is obtained by multiplying P_{cons} by the time saved as a result of quicker charging due to improved η_E provided by 2HET. The ON time of the RF source for charging an uncharged 50 mF super-capacitor at the target node up to 3V, respectively via DET, normal 2HET ($P1$) with ORP, and 2HET with distributed beamforming ($P2$) and ORP in the three cases are mentioned in Table IV.

TABLE IV: RF source runtime comparison.

Case	RF source *ON* time or target node charging time T_C (sec)		
	DET	Normal 2HET ($P1$) with ORP	2HET with beamforming ($P2$) and ORP
A	537.0185	479.6894	465.4343
B	306.4518	282.0659	276.9978
C	140.6250	135.5742	131.3924

So, the energy saved is calculated as: $E_{saved} = P_{cons} \times \left[T_C\left(50\text{mF}, 3, P_{r_1}\right) - T_C\left(50\text{mF}, 3, P_T\right)\right]$, where T_C is defined in (9), $P_T = P_{2HET}$ for $P1$, and $P_T = P_{2HET}^{DB}$ for $P2$.

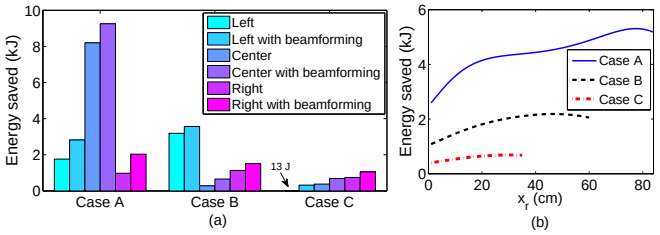

Fig. 12: (a) Energy saving by ORP in 2HET compared to arbitrary placement (left, center, right); (b) Energy saving in 2HET with distributed beamforming compared to DET.

E_{saved} in the two scenarios ($P1$ and $P2$), i.e., without and with distributed beamforming, compared to the three arbitrary relay positions (left, center, and right) are shown in Fig. 12(a). Also the energy savings in 2HET with distributed beamforming with respect to DET as a function of relay position is shown in Fig. 12(b) for the three values of x_0. The results in Figs. 12(a) and (b) indicate that, the energy saving is larger when x_0 increases. Fig. 12 also indicate that, the ORP is strongly dependent on x_0. A relative look at the Figs. 12(a) and (b) further reveal that, ORP gain with respect to arbitrarily positioned relay in 2HET can be even higher than the gain with respect to DET. For example, with $x_0 = 100$ cm the ORP with beamforming achieves an energy saving up to 9 kJ with respect to the relay placement at the center (non-shadowing), whereas the maximum gain compared to DET is about 5 kJ. This is because, an arbitrarily positioned relay in 2HET can cause destructive interference at the destination, resulting in even poorer performance than DET.

TABLE V: Optimal relay placement results.

Case		Optimal Position $(x_r, y_r - y_0)$ (cm)	P_{DET} (mW)	Maximum P_{2HET} (mW)	Efficiency η_E (%)	Energy saved (J)
A	$P1$	$(61.08, 4.7\times10^{-10})$	0.4190	0.4690	11.94	4252.10
	$P2$	(76.41, 0)		0.4834	15.38	5309.40
B	$P1$	$(34.49, 8.9\times10^{-11})$	0.7342	0.7977	8.65	1808.70
	$P2$	(45.70, 0)		0.8123	10.63	2184.60
C	$P1$	$(3.86, 4.9\times10^{-12})$	1.6188	1.6799	3.77	374.62
	$P2$	(29.05, 0)		1.7340	7.12	684.78

Table V shows the optimal relay positions in the two ORP problems (i.e., without/with distributed beamforming), the harvested power at the target node, and the percentage energy transfer improvements with 2HET. The optimal value of y_r in normal 2HET (without beamforming) comes out to be nearly the same as that with beamforming. This is due to very low relay transmit power (5 dBm) of the Mica2 mote (relay transmitter) compared to the RF source (20 dBm) and very low duty cycle around 4 %. This causes the relay's contribution in P_{2HET} to be dominated by path loss rather than destructive interference. However, this is not true in general. With improved RF harvesting circuits [23] and motes with lower active state consumption and higher transmit power comparable to that of the RF source, destructive interference can be a major factor in determining the ORP. For instance, we consider the following specific improved system parameters: (a) *transmit power of relay increased from* 5 *dBm to* 20 *dBm;* (b) *RF-to-DC rectification efficiency improved by* 30% *(cf. Fig. 5(b));* (c) *relay antenna gains increased from* 6.1 *dBi to* 9.1 *dBi;* (d) *reduced ON (energy transmission) state current consumption from* 30 *mA to* 9 *mA.*

TABLE VI: ORP with improved system parameters.

Optimal relay placement for $P1$		
Case	Optimal Position $(x_r, y_r - y_0)$ (cm)	P_{2HET} (mW)
A	(84, 6.11)	3.1629
B	(59, 6.57)	2.9248
C	(34, 11.08)	3.8267

With these improved futuristic system parameters, ORP results for the three cases considered are given in Table VI. The numerical results obtained in Table VI indicate that ORP in $P1$ can have $y_r - y_0 > 0$, and not always necessarily $y_r \approx y_0$.

VII. Concluding Remarks

In this paper, we presented a novel optimization problem in 2HET for improving RFET efficiency. We showed how distributed beamforming can further improve the efficiency by introducing controlled phase shift between the local oscillators at the RF source and the relay node. As the two optimization problems presented are nonconvex and highly nonlinear, we presented a global optimization algorithm that provide fast and efficient convergence to the ϵ-global optimal solution. We also proved that ORP problem in 2HET using distributed beamforming is pseudo-concave for the commercially available RF energy harvesters and antennas from Powercast. Through numerical examples, we showed the effectiveness of the proposed algorithm and the significance of placing the relay node optimally as opposed to 2HET with arbitrary relay

positions, in terms of improved RFET efficiency and energy saving. Numerical results show that, 2HET performance gain over DET increases with end-to-end RFET distance – which is encouraging for MHET as the energy harvesting technology advances. With ORP and beamforming, up to 25% gain against arbitrarily-positioned relay in 2HET (as opposed to 15% gain against DET) at 100 cm RFET distance demonstrates the criticality of ORP, because it proves that due to destructive interference 2HET performance can be even poorer than DET unless the relay is optimally positioned.

In future, we intend to consider the ORP for RFET in more than two-hops by using multiple energy harvesting relays. Multi-relay environment is more challenging, as it needs added inter-relay cooperation besides distributed beamforming with the RF source. We also plan to consider the shadowing and multi-path effects in a more enhanced channel model by incorporating the available channel state information.

REFERENCES

[1] S. De and R. Singhal, "Toward uninterrupted operation of wireless sensor networks," *IEEE Computer Mag.*, vol. 45, no. 9, pp. 24–30, Sep. 2012.

[2] M. Watfa, H. Al-Hassanieh, and S. Selman, "Multi-hop wireless energy transfer in WSNs," *IEEE Commun. Lett.*, vol. 15, no. 12, pp. 1275–1277, Dec. 2011.

[3] L. Xiang, J. Luo, K. Han, and G. Shi, "Fueling wireless networks perpetually: A case of multi-hop wireless power distribution," in *Proc. IEEE Int. Symp. Personal Indoor and Mobile Radio Commun. (PIMRC)*, London, UK, Sep. 2013, pp. 1994–1999.

[4] T. Rault, A. Bouabdallah, and Y. Challal, "Multi-hop wireless charging optimization in low-power networks," in *Proc. IEEE GLOBECOM*, Atlanta, GA, USA, Dec. 2013, pp. 462–467.

[5] K. Kaushik, D. Mishra, S. De, S. Basagni, W. Heinzelman, K. Chowdhury, and S. Jana, "Experimental demonstration of multi-hop RF energy transfer," in *Proc. IEEE Int. Symp. Personal Indoor and Mobile Radio Commun. (PIMRC)*, London, UK, Sep. 2013, pp. 538–542.

[6] D. Mishra, K. Kaushik, S. De, S. Basagni, K. Chowdhury, S. Jana, and W. Heinzelman, "Implementation of multi-path energy routing," in *Proc. IEEE Int. Symp. Personal Indoor and Mobile Radio Commun. (PIMRC)*, Washington D.C., USA, Sep. 2014.

[7] A. Kurs, A. Karalis, R. Moffatt, J. Joannopoulos, P. Fisher, and M. Soljacic, "Wireless power transfer via strongly coupled magnetic resonances," *Science*, vol. 317, no. 5834, pp. 83–86, July 2007.

[8] R. Zhang and C. K. Ho, "MIMO broadcasting for simultaneous wireless information and power transfer," *IEEE Trans. Wireless Commun.*, vol. 12, no. 5, pp. 1989–2001, May 2013.

[9] J. Laneman, D. Tse, and G. W. Wornell, "Cooperative diversity in wireless networks: Efficient protocols and outage behavior," *IEEE Trans. Inf. Theory*, vol. 50, no. 12, pp. 3062–3080, Dec. 2004.

[10] S. Ikki, M. Uysal, and M. Ahmed, "Joint optimization of power allocation and relay location for decode-and-forward dual-hop systems over nakagami-m fading channels," in *Proc. IEEE GLOBECOM*, Honolulu, HI, USA, Nov. 2009.

[11] S. Ikki and S. Aissa, "A study of optimization problem for amplify-and-forward relaying over weibull fading channels with multiple antennas," *IEEE Commun. Lett.*, vol. 15, no. 11, pp. 1148–1151, Nov. 2011.

[12] C. Kundu and R. Bose, "Joint optimal power allocation and relay location for amplify-and-forward multihop relaying over lognormal channel," in *Proc. IEEE VTC Spring*, Dresden, Germany, June 2013.

[13] I. Krikidis, "Simultaneous information and energy transfer in large-scale networks with/without relaying," *IEEE Trans. Commun.*, vol. 62, no. 3, pp. 900–912, Mar. 2014.

[14] D. Michalopoulos, H. Suraweera, and R. Schober, "Relay selection for simultaneous information transmission and wireless energy transfer: A tradeoff perspective," *IEEE J. Sel. Areas Commun.*, vol. PP, no. 99, Jan. 2015.

[15] A. Nasir, X. Zhou, S. Durrani, and R. Kennedy, "Relaying protocols for wireless energy harvesting and information processing," *IEEE Trans. Wireless Commun.*, vol. 12, no. 7, pp. 3622–3636, July 2013.

[16] Z. Ding, S. Perlaza, I. Esnaola, and H. Poor, "Power allocation strategies in energy harvesting wireless cooperative networks," *IEEE Trans. Wireless Commun.*, vol. 13, no. 2, pp. 846–860, Feb. 2014.

[17] R. Mudumbai, G. Barriac, and U. Madhow, "On the feasibility of distributed beamforming in wireless networks," *IEEE Trans. Wireless Commun.*, vol. 6, no. 5, pp. 1754–1763, May 2007.

[18] F. Quitin, M. M. U. Rahman, R. Mudumbai, and U. Madhow, "A scalable architecture for distributed transmit beamforming with commodity radios: Design and proof of concept," *IEEE Trans. Wireless Commun.*, vol. 12, no. 3, pp. 1418–1428, Mar. 2013.

[19] X. Chen, X. Wang, and X. Chen, "Energy-efficient optimization for wireless information and power transfer in large-scale MIMO systems employing energy beamforming," *IEEE Wireless Commun. Lett.*, vol. 2, no. 6, pp. 667–670, Dec. 2013.

[20] D. Jenn, "Transmission equation for multiple cooperative transmitters and collective beamforming," *IEEE Antennas Wireless Propag. Lett.*, vol. 7, pp. 606–608, Aug. 2008.

[21] C. S. Adjiman, S. Dallwig, C. A. Floudas, and A. Neumaier, "A global optimization method, α-BB, for general twice-differentiable constrained NLPs–I. Theoretical advances," *Computers & Chemical Engineering*, vol. 22, no. 9, pp. 1137–1158, Aug. 1998.

[22] Powercast. [Online]. Available: http://www.powercastco.com.

[23] P. Nintanavongsa, U. Muncuk, D. Lewis, , and K. Chowdhury, "Design optimization and implementation for RF energy harvesting circuits," *IEEE J. Emerg. Sel. Topics Circuits Syst.*, vol. 2, no. 1, pp. 24–33, Mar. 2012.

[24] J. Ruze, "Physical Limitations on Antennas," *MIT Research Laboratory of Electronics, Tech. Rep. 248*, Oct. 30 1952.

[25] C. A. Floudas, *Deterministic Global Optimization: Theory, Methods and Applications*. Dordrecht: Kluwer Academic Publishers, 2000.

[26] C. D. Maranas and C. A. Floudas, "Global minimum potential energy conformations of small molecules," *J. Global Optim.*, vol. 4, no. 2, pp. 135–170, Mar. 1994.

[27] M. J. Powell, "Convergence properties of algorithms for nonlinear optimization," *Siam Review*, vol. 28, no. 4, pp. 487–500, Dec. 1986.

[28] A. D. Belegundu and T. R. Chandrupatla, *Optimization concepts and applications in engineering*. Cambridge University Press, 2011.

[29] E. W. Weisstein, "Least Squares Fitting–Polynomial," From MathWorld – A Wolfram Web Resource. [Online]. Available: http://mathworld.wolfram.com/LeastSquaresFittingPolynomial.html

[30] D. Hooper, J. Coughlan, and M. R. Mullen, "Structural equation modeling: Guidelines for determining model fit," *Electronic J. Business Research Methods*, vol. 6, no. 1, Apr. 2008.

[31] M. S. Bazaraa, H. D. Sherali, and C. M. Shetty, *Nonlinear Programming: Theory and Applications*. New York: John Wiley and Sons, 2006.

Deepak Mishra [S'13] received his B.Tech degree in Electronics and Communication Engineering from Guru Gobind Singh Indraprastha University, Delhi, India, in 2012. He is currently pursuing the Ph.D. degree from the Department of Electrical Engineering, IIT Delhi, India. His research interests include energy harvesting cooperative networks, wireless rechargeable sensor networks and mobility management in ad hoc sensor networks. He is a student member of IEEE and IEEE Communications Society.

Swades De [S'02-M'04-SM'14] received the Ph.D. degree in Electrical Engineering from the State University of New York at Buffalo, NY, USA, in 2004. He is currently an Associate Professor in the Department of Electrical Engineering, IIT Delhi, India. His research interests include performance study, resource efficiency in wireless networks, broadband wireless access, and communication and systems issues in optical networks. Dr. De currently serves as an associate editor for the IEEE Communications Letters and the Springer Photonic Network Communications journal. He is a senior member of the IEEE, IEEE Communications Society, and IEEE Computer Society, and a member of the IEICE.